CENTRO DE INVESTIGACION EN MATERIALES AVANZADOS S.C.
MIGUEL DE CERVANTES 120,COMPLEJO IND. CHIHUAHUA
CIM941025MJ1

No. REQUISICIÓN
221054

FO-CON-03 REQUISICIÓN DE BIENES, ARRENDAMIENTOS Y SERVICIOS
(REQ. CAPTURADA USUARIO)

Área requirente	SUBSEDE DURANGO	**Nombre del Proyecto**	DESARROLLO DE UN CALENTADOR SOLAR DE AIRE DE	**Fecha Elaboración**	29/09/2022
Solicita	00427 - NAJERA TREJO MARIO	**Lugar entrega**	CIMAV SUBSEDE DURANGO, CALLE CIMAV 110, EJIDO ARROYO SECO, 34147 DURANGO, DGO.	**Fecha requerida**	29/09/2022
				Fecha impresión	29/09/2022

#	PROYECTO	PART	CUCOP	ARTICULO	DESCRIPCION	UM	CANTIDAD SOLICITADA	PRECIO UNITARIO	IMPORTE
1	24024	21502		21502.0006	ARTICULO DE REVISTA , |, | , | PAGO DE PUBLICACION DE ARTICULO EN REVISTA MDPI PAGO EN FRANCOS (T.C. 20.64)	PZA	1.000	47,472.00	47,472.00

ANEXOS NO	**EXISTENCIA ALMACEN** NO	**ANTICIPO** NO	**PLURIANUALIDAD** NO **MESES** 0	**PAÍS DE ORIGEN** SUIZA	
CAPACITACIÓN NO	**REGISTRO SANITARIO** NO		**PENAS CONVENC.** SI **PORC.%** 0.2	**TIEMPO FABRICACIÓN** ,	Subtotal 47,472.00
NORMAS INSPECCIÓN NO			**METODOS PRUEBA** NO		
TIPO GARANTÍA NO APLICA	**PORC. GARANTÍA** 0 %		**COND. ENTREGA** EN UNA SOLA EXHIBICIÓN		I.V.A. 0.00
TIPO GARANTÍA 2 NO APLICA	**PORC. GARANTÍA 2** 0 %		**COND. PAGO** SEGÚN REFERENCIA		Total 47,472.00
OBSERVACIONES ,			**SUFICIENCIA PRESUPUESTAL** SI		

NAJERA TREJO MARIO	MARTIN DOMINGUEZ IGNACIO RAMIRO	PRESUPUESTOS
SOLICITANTE	RESPONSABLE PROYECTO	PRESUPUESTO AUTORIZADO

CENTRO DE INVESTIGACION EN MATERIALES AVANZADOS S.C.
MIGUEL DE CERVANTES 120,COMPLEJO IND. CHIHUAHUA
CIM941025MJ1

No. REQUISICIÓN
221054

FO-CON-02 CONSTANCIA DE EXISTENCIAS DE BIENES EN ALMACEN

Área requirente SUBSEDE DURANGO
Solicita 00427 - NAJERA TREJO MARIO
Fecha Elaboración 29/09/2022
No. de Requisición 221054

ARTICULO	PART	CUCOP	DESCRIPCIÓN DE BIENES	UM	EXISTENCIA	FECHA DE ULTIMA ENTRADA	EXISTENCIA DISPONIBLE	BIENES ASIGNADOS	OBSERVACIONES EN CASO DE QUE LAS EXISTENCIAS SE ENCUENTREN ASIGNADAS	ROTACIÓN DE INVENTARIO
21502.0006	21502		ARTICULO DE REVISTA , | , | . | PAGO DE PUBLICACION DE ARTICULO EN REVISTA MDPI PAGO EN FRANCOS (T.C. 20.64)	PZA	Ø					

cimav Centro de Investigación en Materiales Avanzados, S.C.
NIVEL DE INVENTARIO DE UNIDAD DURANGO
29 SET. 2022
BIENES EN EL ALMACEN
CANTIDAD: Ø

Nota: Esta constancia, sólo es válido con el sello del almacén

OBJETIVO:

Garantizar que el área requirente verificó en el almacen el nivel de existencia de los bienes que requiere y en su caso justificar la adquisición de los mismos como resultado de las estrategias determinadas por la dependencia o entidad para el adecuado control de los inventarios (artículo 27 del Reglamento de la Ley de Adquisiciones, Arrendamientos y Servicios del Sector Publico)

NAJERA TREJO MARIO
SOLICITANTE

Jose Daniel Bayona Ch.
RESPONSABLE DE ALMACÉN

Naghelli Ortega-Avila
Centro de Investigación en Materiales Avanzados S.C.
Av. Miguel de Cervantes 120, Complejo Industrial Chihuahua
Chihuahua 31136
Mexico

PROFORMA INVOICE

MDPI
St. Alban-Anlage 66
4052 Basel
Switzerland
Tel.: +41 61 683 77 34
E-Mail: billing@mdpi.com
Website: www.mdpi.com
VAT nr. CHE-115.694.943

Date of Invoice:	28 September 2022
Manuscript ID:	applsci-1958428-Proforma
Invoice Number:	1958428
Your Order:	by e-mail (naghelli.ortega@cimav.edu.mx) on 22 September 2022
Article Title:	"Thermal performance analysis of a double-pass solar air collector: A CFD approach"
Name of co-authors:	Irving A. Chávez-Bermúdez, Norma A. Rodríguez-Muñoz, Eduardo Venegas-Reyes, Loreto Valenzuela and Naghelli Ortega-Avila Additional Author Information
Terms of payment:	5 days
Due Date:	3 October 2022
License:	CC BY

Description	Currency	Amount
Article Processing Charges	CHF	2 300.00
Subtotal without VAT	CHF	2 300.00
VAT (0%)	CHF	0.00
Total with VAT	**CHF**	**2 300.00**

Accepted Payment Methods

1. Online Payment by Credit Card in Swiss Francs (CHF)

Please visit https://payment.mdpi.com/1896263 to pay by credit card. We accept payments in Swiss Francs (CHF) made through VISA, MasterCard, Maestro, American Express, Diners Club, Discover and China UnionPay.

2. Paypal in Swiss Francs (CHF)

Please visit https://payment.mdpi.com/payment/paypal and enter the payment details. Note that the fee for using Paypal is 5% of the invoiced amount.

3. Wire Transfer in Swiss Francs (CHF)

Important: **Please provide the Manuscript ID (applsci-1958428) when transferring the payment**

Payment in CHF must be made by wire transfer to the MDPI bank account. Banks fees must be paid by the customer for both payer and payee so that MDPI can receive the full invoiced amount.

IBAN: CH48 0483 5160 4356 5100 0
Beneficiary's Name: MDPI AG
Beneficiary's Address: St. Alban-Anlage 66, CH-4052 Basel, Switzerland
Bank Account Number (CHF, Swiss Francs Account for MDPI): 0060-1604356-51
Bank Name: Credit Suisse
Bank Address: Credit Suisse, St. Alban-Graben 1-3, Postfach 2560, CH-4002 Basel, Schweiz
SWIFT code (Wire Transfer Address): CRESCHZZ80A
Clearing number: 4835

For detailed payment instruction, or for more alternative payment methods, visit the website at https://www.mdpi.com/about/payment.

Thank you for choosing MDPI.

× +

Journals Topics Information Author Services Initiatives About naghelli.ortega@gmail.com My Profile Logout Submit

collapse all Submit Manuscript

⌄User Menu

- Home
- Manage Accounts
- Change Password
- Edit Profile
- Logout

⌄Submissions Menu

- Submit Manuscript
- Display Submitted Manuscripts
- Display Co-Authored Manuscripts
- English Editing
- Discount Vouchers
- Invoices
- LaTex Word Count

⌄Reviewers Menu

- Reviews
- Volunteer Preferences
- Recruiting Reviewers

Author Dashboard

Papers in progress

collapse(1)

Manuscript-ID	Title	Section/Special Issue/Topic	Status	Submission Date
applsci-1958428	Thermal performance analysis of a double-pass solar air collector: A CFD approach	**Topic:** Advances in Renewable Energy and Energy Storage	Under review	2022-09-22

Disclaimer Terms and Conditions Privacy Policy

Centro de Investigación en Materiales Avanzados S. C.

FECHA: 14 de septiembre de 2022

ASUNTO: SOLICITUD DE COTIZACIÓN

A quien corresponda:
MDPI
ST ALBAN-ANLAGE 66, 4052 BASEL, SWITZERLAND

El **Cimav**, como Centro de Investigación del Gobierno Federal, requiere para sus actividades de suministro, arrendamiento y/o prestación de servicios, mismas que se encuentran reguladas por la Ley de Adquisiciones, Arrendamientos y Servicios del Sector Público (LAASSP) y su Reglamento, obtener información para contratar bajo las mejores condiciones disponibles para el Estado.

En este sentido y en terminos de lo previsto en el artículo 2 fracción X de la LAASSP, su representada ha sido identificada por este ente público, como un posible prestador de servicio y/o proveedor.

Por lo antes mencionado y con el objeto de conocer: a).- la existencia bienes, arrendamientos o servicios a requerir en las condiciones que se indican; b).- posibles proveedores a nivel nacional o internacional; c).- el precio estimado de lo requerido, y d).- la capacidad de cumplimiento de los requisitos de participación, nos permitimos solicitar su valioso apoyo a efecto de proporcionarnos la cotización de los bienes y/o servicios y/o arrendamientos descritos en la última hoja de este documento y/o en el o los documentos anexos.

Dicha cotización se requiere que la remita en documento de la empresa, debidamente firmada por persona facultada, a la siguiente dirección:

Calle CIMAV #110,
Ejido Arroyo Seco
Durango, Dgo. México. C.P. 34147

Y que sea dirigida a nombre de: **NAJERA TREJO MARIO**.

Mucho agradeceré que en su respuesta se incluya: *Lugar y fecha de cotización y vigencia de la misma.*

Para el caso de dudas, comentarios y/o aclaraciones, remitirlas al correo: **mario.najera@cimav.edu.mx**

La fecha límite para presentar la cotización es el: **25 de septiembre de 2022**

Favor de enviar acuse de recibo de esta solicitud al correo electrónico a: **alonso.carrasco@cimav.edu.mx**

NOTA: Vencido el plazo de recepción de cotizaciones, el **Cimav** con fundamento en lo previsto en el artículo 26 de la LAASSP, se definirá el procedimiento a seguir para la contratación, el cual puede ser: LICITACIÓN PÚBLICA, INVITACIÓN A CUANDO MENOS TRES PERSONAS y/o ADJUDICACIÓN DIRECTA, mismo que se informará a las personas que presentaron su cotización.

Este documento no genera obligación alguna para el centro.

(Para efectos de control interno, en el caso de no recibir respuesta o manifestar un inconveniente o imposibilidad, se procederá a hacer la anotación respectiva en nuestros registros, circunstancias que deberán ser consideradas al momento de definir el tipo de procedimiento de contratación)

PARA FORMULAR SU COTIZACIÓN, SE DEBERA CONSIDERAR LOS SIGUIENTES ASPECTOS:

Datos que en su caso, se deben proporcionar para que el destinatario de la solicitud conteste:

1.- Los datos de los bienes, arrendamientos o servicios a cotizar los cuales se especifican en el anexo.

2.- Condiciones de entrega:

- o Nota: en caso de que la requisición sea sometida ante el Comité de Adquisiciones, la fecha de entrega deberá considerar adicionalmente, un lapso de 6 días naturales posteriores a la celebración de la Sesión.
- o En una sola exhibición con fecha de entrega al: 31 de octubre de 2022.
- o El lugar de entrega será: Virtual a través del portal de la revista JCR

3.- Considerar en su cotización que el pago es a los 20 días naturales posteriores a la entrega de la factura, previa entrega de los bienes o prestación de los servicios a satisfacción.

4.- Señalar en su caso, el porcentaje del anticipo: 0

5.- El porcentaje de garantía de cumplimiento será del 0%.

6.- Penas convencionales por atraso en la entrega de bienes y/o servicios y deducciones por incumplimiento parcial o deficiente serán del 5 al millar (0.005) para bienes y 2 al millar (0.002) para servicios.

7.- En su caso, los métodos de prueba que empleará el ente público para determinar el cumplimiento de las especificaciones solicitadas.

- o Normas que deben de cumplirse.
- o Registros Sanitarios o Permisos Especiales, en su caso.

8.- Origen de los bienes (nacional o país de importación) y nacionalidad de los posibles proveedores.

9.- En caso de bienes de importación la moneda en que cotiza.

10.- En caso de que el proceso de fabricación de los bienes requeridos sea superior a 60 días, señale el tiempo que correspondería a su producción.

11.- En su caso, especificar si el costo incluye:

- o Instalación.
- o Capacitación.
- o Puesta en marcha.

12.- Otras garantías que se debe considerar, indicar el o los tipos de garantía, o de responsabilidad civil señalando su vigencia.

Descripción con las especificaciones técnicas y requisitos de calidad, cantidad y oportunidad del o los bienes, arrendamiento y/o servicios a contratar:

Publicación de artículo en revista JCR de MDPI - Manuscript ID: applsci-1958428 (Entregable del proyecto)

applied sciences

MDPI

Article

Thermal performance analysis of a double-pass solar air collector: A CFD approach

Irving A. Chávez-Bermúdez [1], Norma A. Rodríguez-Muñoz [2], Eduardo Venegas-Reyes [3], Loreto Valenzuela [4] and Naghelli Ortega-Avila [2,*]

[1] Centro de Investigación en Materiales Avanzados, Calle CIMAV 110, Ejido Arroyo Seco, Durango 34147, México; irving.chavez@cimav.edu.mx
[2] CONACYT-Centro de Investigación en Materiales Avanzados, Calle CIMAV 110, Ejido Arroyo Seco, Durango 34147, México; norma.rodriguez@cimav.edu.mx
[3] Instituto Mexicano de Tecnología del Agua, Paseo Cuauhnáhuac 8532, Progreso, Jiutepec, Morelos 62550, México; eduardo_venegas@tlaloc.imta.mx
[4] CIEMAT-Plataforma Solar de Almería, Ctra. Senés, 04200 Tabernas, Almería, Spain; loreto.valenzuela@psa.es
* Correspondence: naghelli.ortega@cimav.edu.mx

Featured Application: The developed solar air heater can be applied in drying and space heating applications from 50 °C to 90 °C. The solar collector could be modular, so it can be coupled to a variety of processes.

Abstract: Solar air heaters can reduce climate change by replacing conventional fossil fuels-burning technologies in drying and space heating applications. Concentrating solar technologies, such as compound parabolic concentrators, allow air temperatures up to 120 °C; however, it is desirable to improve their heat transfer to reduce the space requirements for their installation. In this work, a parabolic concentrator composed of a flat receiver designed to recover heat from the cover-receiver-reflectors cavity is analyzed, operating it as a U-shape double pass solar heater. With this operation, first, the air flows through the cavity, and then it is incorporated into the duct, where the dominant heat gain occurs due to the capture of solar radiation. Thus, four input-output configurations in the cavity were modeled through dynamic simulations to determine the influence of the inlet and outlet air flow positions on the solar concentrator outlet temperature. It was found that the configuration with the top inlet and the top outlet is optimal since a temperature increase of up to 38.5 K and an efficiency of 72 % can be obtained. Finally, the incorporation of the double pass allows increasing the concentrator outlet temperature up to 39 %, showing that this appropriate and relatively simple strategy can be implemented to improve the thermal performance of solar air collectors.

Keywords: solar energy; CPC; solar heating; solar drying; industrial process; solar air heater; space heating

Citation: Lastname, F.; Lastname, F.; Lastname, F. Title. *Appl. Sci.* **2022**, *12*, x. https://doi.org/10.3390/xxxxx

Academic Editor: Firstname Lastname

Received: date
Accepted: date
Published: date

1. Introduction

Air heating is used for various applications, such as heating and air conditioning of buildings or drying of food and industrial products, among others. Air can be heated with electric heaters or by directly burning fuels such as gas; however, their use implies the emission of greenhouse gases and their consequent contribution to climate change. One way to minimize fossil fuel burning is to use solar collectors to directly heat the air, ranging from flat-plate collectors to solar concentrators.

According to the International Energy Agency, 985 MW_{th} solar air collectors were installed by the end of 2020, and the global market was around 12 MW_{th} [1]. As of March 2022, 41 solar air collector systems producing solar process heat are registered, with a cumulative capacity of 6 MW_{th} [1]. Thus, the direct application of solar collectors for air heating is low due to the boost that low fossil fuel prices give to using conventional technologies [2], so it is essential to develop reliable and economical efficient solar air heating technologies. Flat-plate solar collectors are recommended for temperatures below 70 °C because of their ease of manufacture and operation. For higher temperatures, it is necessary to use some solar concentrating technology, such as compound parabolic concentrators (CPCs), which allow fluid heating temperatures up to 120 °C, depending on their design, and are easy to operate and maintain.

However, to ensure good efficiency of CPCs, it is necessary to perform an optimal optical design and minimize thermal losses or improve heat transfer. Strategies to reduce convection losses in the receiver of a solar collector include using evacuated tubes or filling the CPC cavity with gases such as Argon and Krypton [3,4], which are denser gases and have lower thermal conductivity than air or even applying vacuum throughout the cavity [5]. In contrast, double absorbers have been proposed to reduce conduction losses [6].

In other technologies, such as flat-plate solar air heaters, it has been proposed to increase the heat transfer rate by incorporating multiple passages, including extended surfaces, artificial roughness, and packed mesh [7]. This multi-pass strategy is used in hybrid CPCs (PV/T) to cool the photovoltaic cells on the flat-plate receiver with fins on the back side [8].

In the general design of solar collectors, computational fluid dynamics (CFD) tools can be used to reliably estimate their thermo-hydraulic performance before building them, saving time and resources. Several analyses of solar collectors by computational fluid dynamics (CFD) can be found in the literature, both for liquid and air heating. Thus, Mekahlia et al. (2020) determined the influence of the thickness and number of transparent covers to reduce the heat losses of a flat-plate solar collector [9], and Pawar and Sobhansarbandi (2020) modeled an evacuated heat-pipe solar collector with and without integrated phase change materials as a thermal storage medium [10]. In the particular case of solar air collectors, Singla et al. (2022) analyzed an evacuated tube collector with ribs of different roughness [11], while Ammar et al. (2020) performed a three-dimensional CFD model to optimize the design of a solar air collector with extended surface area by a different number of rectangular fins [12]. In addition, they analyzed the effect of adding a selective surface on the absorber.

Regarding the analysis of CPC collectors, Li et al. (2013) analyzed by CFD the thermal behavior of an evacuated tube collector as a receiver of a compound parabolic concentrator, and the simulation was validated with experimental data [13]. Barrón-Díaz et al. (2021) performed the numerical simulation of CPCs with tubular receivers, with and without fins, for residential water heating [14]. This study focused on the ray-tracing analysis of radiation and heat transfer by coupled finite element and CFD methods. In addition, Yuan et al. (2020) developed two simplified computational fluid dynamics models to determine the temperature and velocity distribution in two almost identical parabolic tube-receiver CPCs [15]. One had a transparent ETFE sheet around the receiver to reduce convective heat losses. The models included the reflector, receiver, cover, and back insulating material and allowed analysis of both air movement in the cavity and water movement in the absorber tube. Ray tracing was applied to analyze the radiation distribution on the receiver tube at normal incidence, with a correlation of the absorbed solar energy as a function of the angle along the perimeter of the tube. Both models were experimentally validated, and relative errors of less than 3.7 % in temperature and 1 % in efficiency were obtained.

On the other hand, Antonelli et al. (2016) analyzed the air heat transfer inside the cavity of a collector with a tubular receiver and with a flat-plate receiver and developed some correlations to express the Nusselt over the receiver [16]. Subsequently, Francesconi and Antonelli (2018) performed the numerical analysis of a panel with several tubular receivers CPCs to determine the influence on the thermal efficiency of the number and position of the CPCs along the panel, the use of a second transparent cover, the spacing between collectors and the truncation of the reflectors [17]. For their part, Reddy et al. (2020) performed three-dimensional modeling of a flat-plate receiver CPC to determine the thermal losses in the cavity as a function of its aspect ratio and tilt, the optical properties of the materials, and the absorber and ambient temperatures [18]. To model the internal radiative heat transfer, they used a discrete ordinary radiation model, and for the external one, they established the thermal boundary conditions and emissivity.

As mentioned above, another strategy to improve the efficiency of solar air heating collectors is to increase the number of passes. Thus, Al-Damook et al. (2019) analyzed the effect of double-pass configuration in a solar air heater when operating in concurrent parallel flow, parallel in counterflow, and double U-pass [19]; the latter presented the best thermal performance. Tuncer et al. (2020) analyzed, through CFD simulation, two flat-plate solar collectors for air heating with three and four passes and determined which one had the best performance to evaluate it experimentally [20]. In both solar collectors analyzed, air enters through the lower pass and exits through the upper pass, which has the radiant heat gain. They found that the four-pass collector has a heat gain 3 °C higher than that obtained with the three-pass collector and that the maximum deviation between the CFD model and the experimental results was 10 %. In addition, Mutabilwa and Nwaigwe (2020) performed a CFD analysis of a two-covers, double-pass flat-plate solar collector for air heating, which was validated with experimental results [21]. The air enters through the space between the two covers and returns between the second cover and the absorber plate. The temperatures on the absorber plate obtained with the model had a standard deviation from experimental results between 1.05 K and 4.65 K, while for the cover, it was between 0.1 K and 0.45 K.

Likewise, improved surfaces or novel geometries with multiple passes have been analyzed, such as the work of Desisa and Shekata (2020) [22]; they analyzed the impact of using smooth, rough, and corrugated surfaces in a double-pass flat-plate air solar collector and obtained average thermal efficiencies of 78 %, 62 %, and 90 %, respectively. On the other hand, Singh (2020) determined the performance of double-pass flat-plate air solar collectors with different fin configurations [23]. They varied in size, angle, arrangements (in-line, staggered, and hybrid), and hydraulic diameter. Finally, Kumar et al. (2022) proposed a curved air heater with asymmetric double-pass counterflow turbulators, whose design was determined from CFD analysis by comparing various flow configurations and geometric parameters [24].

Two or more pass technologies have been applied in flat-plate solar collectors to improve their efficiency; however, this strategy has not been applied in CPCs for air heating. This study proposes the CFD analysis of a CPC-type solar air heater with U-shape double-pass airflow. The air first circulates through the trapezoidal cavity contained in the volume formed by the cover, the reflecting walls of the CPC, and the flat-plate receiver and then circulates in counterflow through the receiver's duct interior. The objective of the numerical analysis presented is to test different inlet and outlet configurations in the CPC array to determine how these configurations influence the velocity distribution, outlet temperature, and instantaneous efficiency of the U-shape double-pass CPC solar heater.

Section 2 of this manuscript describes the main characteristics of the U-shape double-pass CPC and the four air inlet/outlet configurations considered in its design. It also defines the mesh design to perform the CFD simulation, the mathematical model for such simulation, the boundary conditions applied in the study, and the methodology followed to estimate the thermal efficiency of the U-shape double-pass CPC. Section 3 includes a summary of the simulation results obtained and their discussion and concludes with a summary of the efficiencies calculated for each of the four configurations analyzed.

2. Materials and Methods

2.1. U-shape double-pass CPC description and physical model

The proposed solar air heater is a variant of the flat-plate receiver Compound Parabolic Concentrator (CPC) conceptualized as a U-shape double-pass heat exchanger. Figure 1a shows the evaluated geometry dimensions and the inlet and outlet positions, whereas, in Figure 1b, the CPC cross-section is shown. The CPC is tilted 24° and consists of a flat-plate receiver, two reflectors, a cover, and a duct. The first pass of the airflow inside the CPC occurs in the cavity formed by the receiver, two reflectors, and the cover, while the second pass is in the duct section. The aperture area where the solar radiation enters the CPC is 0.42 m^2, while the area where it is absorbed is 0.20 m^2.

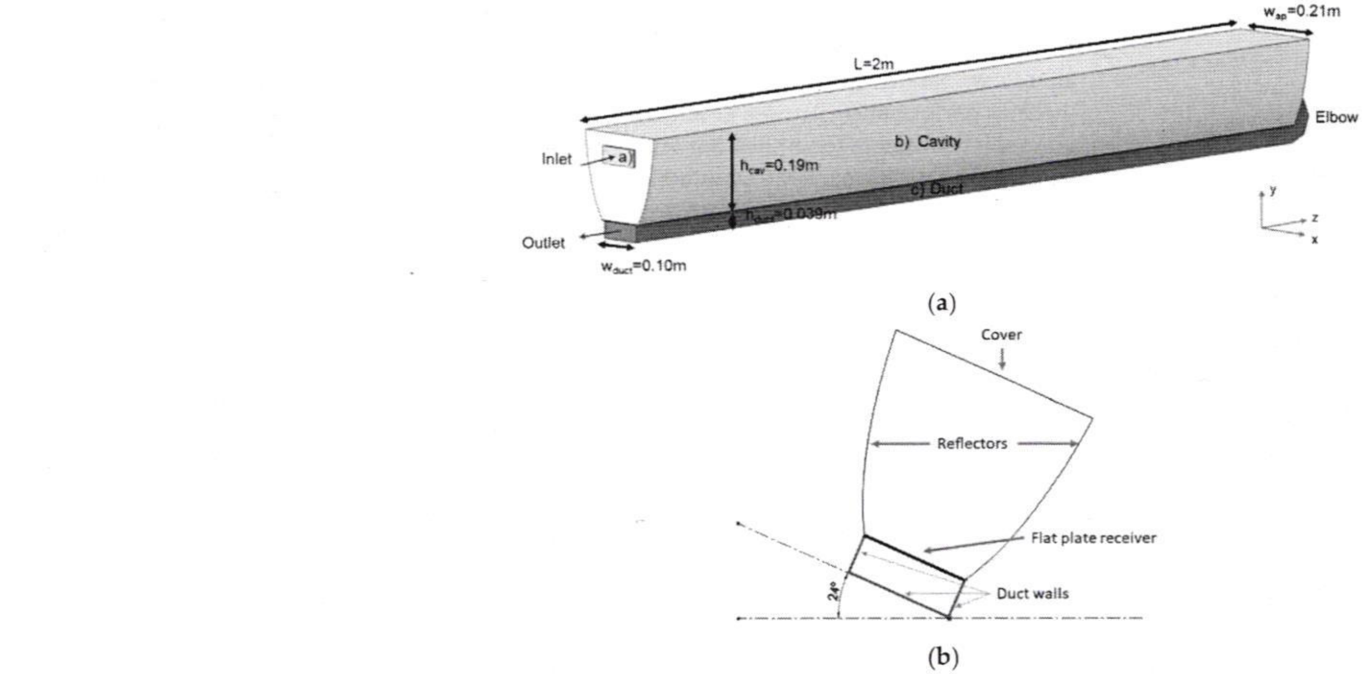

Figure 1. U-shape double-pass CPC solar heater. **(a)** Geometry; **(b)** Cross-section.

The analysis of the position of the air inlet and outlet in the cavity consisted of the study of four configurations which were positioned concerning the height of the cavity (h_{cav}): (a) inlet $\frac{1}{4}h_{cav}$ – outlet $\frac{1}{4}h_{cav}$ (Down-Down), (b) inlet $\frac{1}{4}h_{cav}$ – outlet $\frac{3}{4}h_{cav}$ (Down-Up), (c) inlet $\frac{3}{4}h_{cav}$ – outlet $\frac{3}{4}h_{cav}$ (Up-Up), and (d) inlet $\frac{3}{4}h_{cav}$ – outlet $\frac{1}{4}h_{cav}$ (Up-Down). The air inlet and outlet configurations are shown in Figure 2.

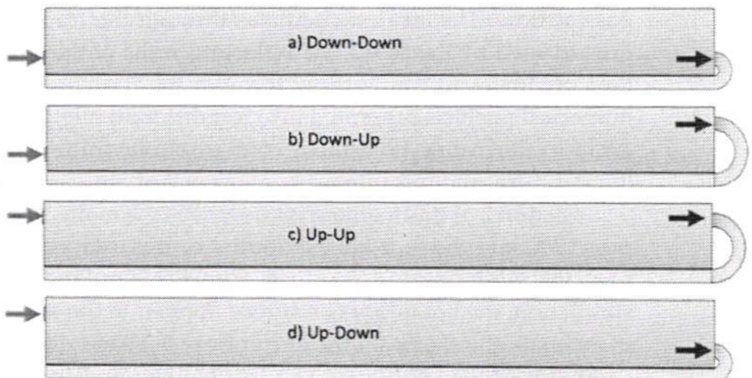

Figure 2. Inlet and outlet studied configurations of U-shape double-pass CPC.

The reflector is made of anodized aluminum, while the other components of the U-shape double-pass CPC, shown in Table 1, were considered in the CFD simulation with a certain thickness to model the conduction. The duct is made of aluminum, and the receiver substrate has a selective surface; this surface has high absorptivity in the solar spectrum and low emissivity in the infrared to avoid losses due to thermal radiation. Finally, the cover is made of solid polycarbonate, and an insulating material (EPS) was considered outside the reflector and the duct to avoid thermal losses from the surface exposed to the environment.

Table 1. Material properties of the U-shape double-pass CPC elements.

Material	Thickness (m)	Thermal conductivity (W/m·K)	Density (kg/m^3)	Specific heat capacity (J/kg·K)
Aluminum (receiver, duct)	0.001	237	2702	903
Expanded polystyrene (EPS) (insulation)	0.050	0.046	14	1210
Polycarbonate (cover)	0.003	0.210	1200	1300

2.1.1. Computational domain

The fluid and solid domains were generated in the SolidWorks 2013 software. The solid domain simulated the absorber plate, while the fluid domain was sectioned into three volumes to facilitate meshing: (a) inlet section, (b) cavity, and (c) elbow-duct.

2.1.2. Mesh

A hexahedral structured mesh was generated according to the proposed computational domain. The near-wall model approach was used to accurately predict the hydrodynamic behavior of the flow and the heat transfer in the system. The method was to implement 15 cells to cover the viscous and buffer sublayer to have accurate results in a reasonable computation time.

The size of the viscous sublayer and the buffer sublayer were calculated for the interval $0.5 < y+ < 5$ using equation 1. In addition, y+ values of 35 and 60 were applied to the turbulent sublayer to carry out the mesh independence study. Through the analysis, the Nusselt number (Nu) varied 0.2 % with y+ values of 0.8 and 0.5.

$$y = \frac{y^{+}\mu}{\rho u_{T}}. \quad (1)$$

The mesh size was verified in the direction of the entrance flow with a cavity mesh refinement in the longitudinal axis (z-axis), as shown in Figure 3. The analysis found that the Nusselt had a variation of 0.089 % from 400 divisions onwards. In Figure 3a, a cross-section of the U-shape double-pass CPC solar heater is shown, with the magnified detail of the mesh in the receiver. Figures 3b1 and 3b2 present the longitudinal section, where the coarse and refined mesh in the cavity are presented.

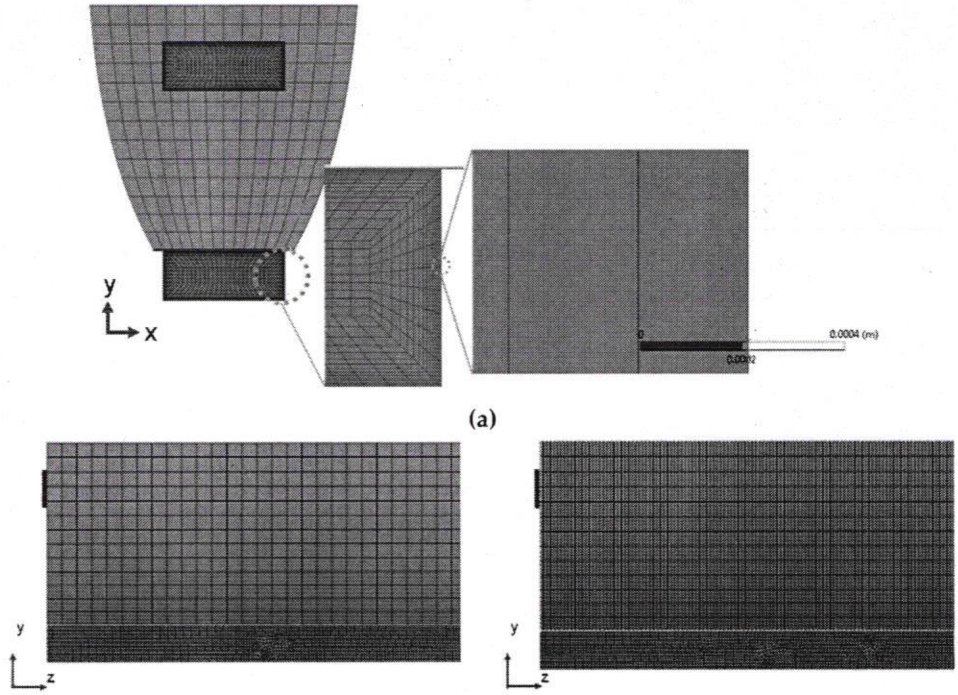

Figure 3. Solar collector mesh. **(a)** Transversal section; **(b1)** coarse mesh in longitudinal section; **(b2)** refined mesh in longitudinal section.

2.2. Mathematical model

The mathematical model had the subsequent considerations for the governing equations: steady state, Newtonian fluid, incompressible flow, and transition turbulence regime; therefore, the governing equations for the U-shape double-pass solar heater are as follows.

$$\frac{\partial \rho}{\partial t} + \nabla \cdot (\rho \vec{v}) = 0, \quad (2)$$

$$\frac{\partial}{\partial t}(\rho \vec{v}) + \nabla \cdot (\rho \vec{v} \vec{v}) = -\nabla p + \nabla \cdot (\bar{\bar{\tau}}) + \rho \vec{g} + \vec{F}, \quad (3)$$

$$\frac{\partial (\rho E)}{\partial t} + \nabla \cdot \left(\vec{v}(\rho E + P)\right) = \nabla \cdot \left(\sum_j h'_j J_j\right). \quad (4)$$

2.2.1. Turbulence model

The turbulence modeling consisted of implementing the Transition SST k-omega model described in equations (5-12). Equation (5) corresponds to the transport equation for intermittency (γ), whereas equations (6) and (7) represent the transition sources $P_{\gamma 1}$ and $E_{\gamma 1}$, respectively; and equations (8) and (9), the destruction/re-laminarization sources $P_{\gamma 2}$ and $E_{\gamma 2}$.

The model was selected due to the required accuracy to predict heat transfer from the absorber plate to the air as the flow was found to be under development ($L_{h,turb} < L_{collector}$) and because the calculated average Reynolds number (Re) was not very high. The average Reynolds number for mass flow rate 1 (0.01 kg/s) was $Re_{cav\text{-}1}$=2,972, and for mass flow rate 2 (0.02 kg/s) was of $Re_{cav\text{-}2}$=5,961. Flows 1 and 2 were selected based on a preliminary analysis using the thermal model described in [25]; among those flows, the best balance between air outlet temperature and thermal efficiency was found. In the calculation of the Reynolds number, the cavity was approximated as a trapezoidal cross-section duct for calculating the hydraulic diameter (D_h).

$$\frac{\partial(\rho\gamma)}{\partial t}+\frac{\partial(\rho U_j\gamma)}{\partial x_j}=P_{\gamma 1}-E_{\gamma 1}+P_{\gamma 2}-E_{\gamma 2}+\frac{\partial}{\partial x_j}\left[\left(\mu+\frac{\mu_t}{\sigma_\gamma}\right)\frac{\partial}{\partial x_j}\right], \quad (5)$$

$$P_{\gamma 1}=C_{a1}F_{length}\rho S[\gamma F_{onset}]^{c_{\gamma 3}}, \quad (6)$$

$$E_{\gamma 1}=C_{e1}P_{\gamma 1}\gamma, \quad (7)$$

$$P_{\gamma 2}=C_{a2}\rho\Omega\gamma F_{turb}, \quad (8)$$

$$E_{\gamma 2}=C_{e2}P_{\gamma 2}\gamma. \quad (9)$$

On the other hand, equation (10) refers to the interaction of the transition model with the SST turbulence model by modifying equation k, where G_k^* and Y_k^* are the original production and destruction terms of the SST model [26].

$$\frac{\partial(\rho k)}{\partial t}+\frac{\partial(\rho k u_i)}{\partial x_j}=\frac{\partial}{\partial x_j}\left(\Gamma_k\frac{\partial k}{\partial x_j}\right)+G_k^*-Y_k^*, \quad (10)$$

$$G_k^*=\gamma_{ef\ f}\tilde{G}_k, \quad (11)$$

$$Y_k^*=\min\big(max(\gamma_{ef\ f},0.1),1.0\big)Y_k. \quad (12)$$

The pressure-based solver with the Coupled scheme was selected, and a second-order spatial discretization scheme was implemented. The gradient evaluation method selected was based on Least Squares Cell-Based, and the high order term relaxation option was used. The pressure factor was adjusted to 0.1, and the Flow Courant Number to 4.

2.2.2. Boundary conditions

The momentum boundary conditions in the walls were considered no-slip stationary with a constant rugosity of 0.5. The thermal boundary conditions modeled the incident solar radiation on the cover and the absorber plate as a heat generation source, calculated using equations (13) and (14).

$$q_c(t)=\left(I(t)\left[\bar{\alpha}_c+\bar{\alpha}_c\bar{\tau}_c\bar{\varrho}_p\varrho_r^{2\langle n\rangle}\right]\frac{A_c}{A_p}\right)/w_c, \quad (13)$$

$$q_p(t)=\left(I(t)\ \ \bar{\tau}_c\varrho_r^{\langle n\rangle}P_g\left[\bar{\alpha}_p+\bar{\alpha}_p\bar{\varrho}_p\bar{\varrho}_c\bar{\varrho}_r^{2<n>}\frac{A_p}{A_c}\right]\frac{A_c}{A_p}\right)/w_p, \quad (14)$$

Where q(t) is the heat generation, I(t) is the solar irradiance, P_g is the gap loss factor (0.96), α is the absorptivity, τ is the transmissivity, ρ is the reflectivity, A_c is the cover area, A_p is the absorber plate area, and w_c and w_g, are the thickness of the cover and plate, respectively. The optical properties of the cover are α_c=0.05, τ_c=0.89 y ρ_c=0.05, the receiver are α_p=0.95 and ρ_p=0.05, and from the reflector ρ_r=0.91.

The heat transfer coefficient from the cover to the environment ($HTC_{c\text{-}a}$) was obtained applying the flow around finite flat-plates methodology reported in [27], while the convection losses of the external walls were calculated using the heat transfer coefficient (HTC_b) correlation proposed by [28]. The heat conduction in the exterior walls of the CPC was modeled as shell conduction, whereas the radiation losses in the cover were calculated with an emissivity value of ε_c=0.81, and the sky temperature (T_s) was calculated with the correlation proposed by Swinbank (equation 15), reported in [29], where T_a refers to the ambient temperature.

Regarding the turbulence parameters, a turbulence intensity of 5 % and a turbulent viscosity ratio of 10 were applied. Table 2 summarizes the parameters of the boundary conditions of the CFD modeling.

$$T_s = 0.0552T_a^{1.5}. \tag{15}$$

Table 2. Boundary conditions considered in the CFD modeling of the U-shape double-pass CPC.

Boundary	Type of boundary	Characteristics
Inlet	Inlet-vent	$T_{ps1,in}$= 298.15 K
Outlet	Mass flow	$\dot{m}_1$= 0.01 kg/s $\dot{m}_2$= 0.02 kg/s
Cover	Wall Mixed (convection, radiation, and heat generation)	q_c= 37.37 kW/m³ $HTC_{c\text{-}a}$= 8.27 W/m·K T_a= 298.15 K T_s= 280.05 K
Bottom duct	Wall Convection Conduction	HTC_b= 0.6 W/m.K
Absorber plate	Wall Heat generation	I= 900 W/m² ε_p= 0.35 q_p= 13,481 kW/m³
Fluid interfaces: - cavity- absorber plate - duct-absorber plate	Coupled wall	-

2.3. Efficiency calculation

The thermal efficiency of the collector is calculated using equation (16):

$$\eta = \frac{Q_u}{A_c I}. \tag{16}$$

The heat transfer of the analyzed solar collector resembles a counterflow heat exchanger, where the cold fluid flows through the cavity (first pass) and the hot fluid flows through the duct (second pass). As the hot current and the cold current are the same air, the useful energy gain must be calculated just in the second pass since the air entering the duct has already gained heat due to its pass through the cavity. Therefore, the useful energy gain of the collector is calculated using equation 17.

$$Q_u = \dot{m}C_{p,avg}\left(T_{ps2,out} - T_{ps2,in}\right). \tag{17}$$

The available test standards for this type of system, such as the ISO 9806 standard [30], do not include an explicit test procedure for air collectors with the proposed design (a double-pass CPC cavity collector). If the classic methodology for calculating the useful energy gain is applied, as is typically done for a flat-plate solar collector, using the temperatures $T_{ps2,out}$ and $T_{ps1,in}$ for the calculation of the CPC efficiency, gross area (A_c), and solar irradiance value (I) as indicated in Eq. 16, values greater than one (η>1) would be obtained for efficiency.

3. Results and discussion

Once the simulation model of the four CPC configurations with different inlet and outlet positions was implemented (Figure 2), simulations were carried out considering the boundary conditions for two different values of mass flow rates to analyze: 0.01 kg/s and 0.02 kg/s. The properties of the materials and the boundary conditions are presented in Tables 1 and 2, respectively. The results of the hydraulic and thermal behavior of the air in the cavity of the CPC for each of these configurations are presented below.

3.1. Hydraulic behavior

Figure 4 shows the velocity streamlines with the two analyzed air mass flow rates (flow 1: 0.01 kg/s and flow 2: 0.02 kg/s). For the four configurations and both flows, a sudden expansion that causes the separation of the main flow is observed. In the configurations with the inlet at the bottom, (a) Down-Down and (b) Down-Up, the separation of the main flow forms an eddy with a mean diameter of $0.22L_{collector}$ at a mean position of z=0.89 m. In configurations with an inlet on the upper side, (c) Up-Up and (d) Up-Down, an eddy is formed in the mean position z=0.68 m with a mean diameter of $0.33L_{collector}$. In addition, it is observed that in the inlet region for the (a) Down-Down and (b) Down-Up configurations, a series of eddies are generated in the upper section of the cavity (z=0.0 m and z=0.42 m). One reason for this is the collector tilt (see Figure 1).

In Figure 4, it is also observed that the outlet position influences the magnitude of the velocity at the entrance to the duct. A higher airflow velocity is seen in configurations with the outlet of the first pass at the bottom section, (a) Down-Down and (d) Up-Down. The pressure increment explains the phenomena due to the sudden air contraction caused by the reduction of the elbow area. Also, a higher mass flow influences the amplitude and turbulence of the eddies found in the first section of the cavity. This phenomenon influences the generation of high-temperature gradients and a more variable thermal map in the transverse direction of the cavity for the 0.01 kg/s air flow rate (see Figure 5). On the contrary, this is not observed with the 0.02 kg/s air flow rate because the higher mass flow rate favors the cooling of the receiver. In all cases and both flows vortices are created in the first quarter of the path, however, in the cases with bottom entry, the turbulence is more disordered at the top, so that in the first quarter of the path, the hot air is not completely transported in the longitudinal direction of the main flow; additionally a second vortex is created so that the uniform flow develops almost halfway. In the top entry cases, the hot air at the top is transported along the entire path, and the uniform flow develops earlier than in the bottom entry cases.

(i)

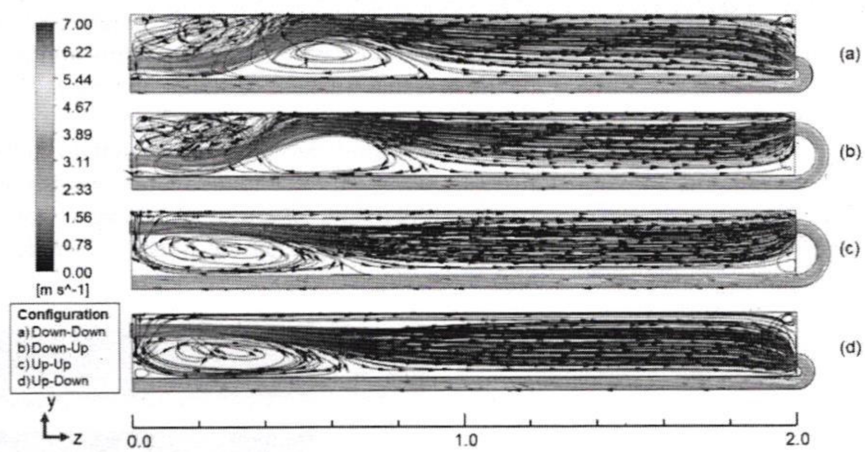

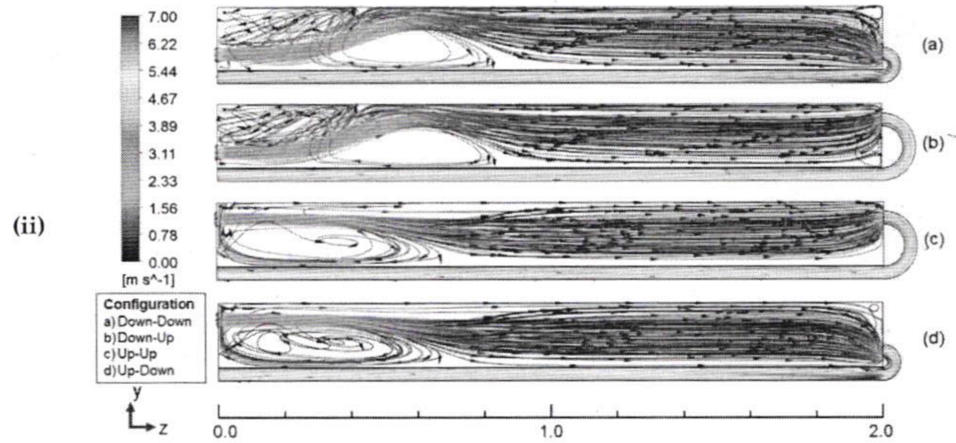

Figure 4. Streamlines at the collector cross-section (**i**) Air mass flow 1: 0.01 kg/s; (**ii**) Air mass flow 2: 0.02 kg/s.

3.2. Thermal behavior

Figure 5 shows the temperature contours of the four analyzed configurations. Here it can be seen that air stratification in the cavity in all configurations and with both mass flow rates (flow 1: 0.01 kg/s and flow 2: 0.02 kg/s) occurs. In flow 1, the elbow inlet temperatures were 314.4 K, 306.8 K, 302.9 K, and 310.8 K for configurations a, b, c, and d, respectively. While with flow 2, these temperatures were 306.4 K, 302.4 K, 302.9 K, and 304.3 K. Lastly, it can be seen that in the two configurations with outlet on top, (b) Down-Up and (c) Up-Up, the stratification causes the entrance of cool air to the elbow, when compared against (a) Down-Down and (d) Up-Down configurations.

A zone with a higher temperature of approximately 335.0 K and 320.3 K for flows 1 and 2 is also observed in position z=0.1 m, in configurations (c) Up-Up and (d) Up-Down. This zone is caused by the presence of the eddy observed in the middle position in Figure 4. In addition, in configurations (b) Down-Up and (c) Up-Up, a zone of hot air is observed at the end of the cavity (z=1.95 m), with similar temperatures. The hot air zone is caused by the presence of small eddies, seen from 0.02 m to 0.06 m, which are formed by the collision of the air at the position z=2.0 m.

In the second step (inside the duct), in configurations (a), (c), and (d), high temperatures are observed close to the plate, contrasting to the temperatures observed in configuration (b). Finally, for a flow of 0.01 kg/s, that heat is extracted from the cavity less efficiently due to the stagnation of the fluid in the extremes, which correspond to the inlet and outlet of the cavity.

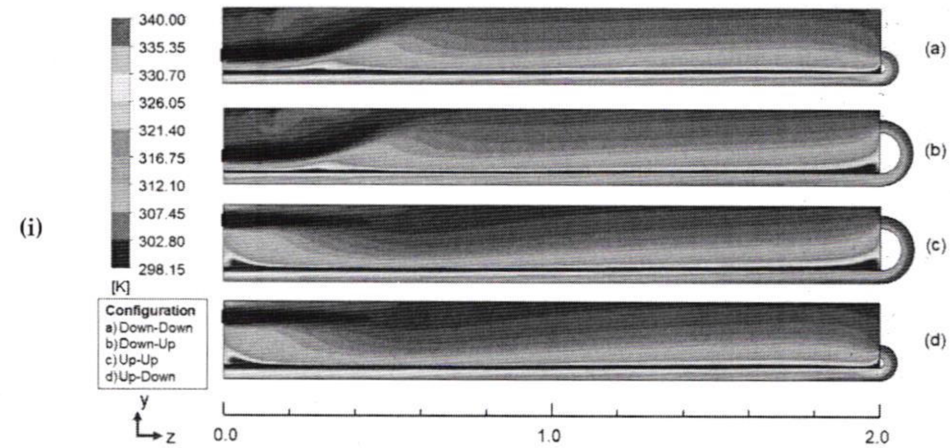

(ii)

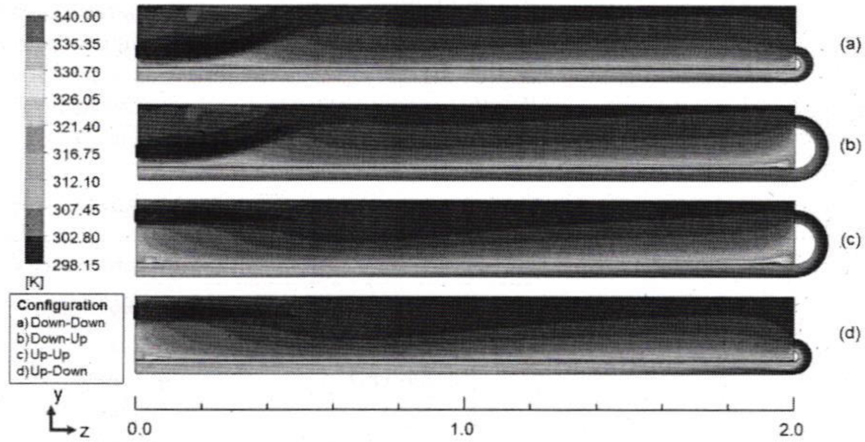

Figure 5. Air temperature contours at the collector cross-section **(i)** Air mass flow 1: 0.01 kg/s; **(ii)** Air mass flow 2: 0.02 kg/s.

Figure 6 shows the four configurations' flat plate receiver temperature contours at flow 1 (0.01 kg/s). When the air enters from below (configurations a and b), it is observed that the air removes heat from the receiver from the position z=0.0 m to z=0.16 m. In contrast, when the air enters from above (configurations c and d), the zones with lower temperatures are displaced from position z=0.22 m to z=0.83 m because the formation of the main eddy helps to remove heat from the receiver. When the air leaves the collector cavity (z=2.0 m), low-temperature zones are generated in the configurations with an outlet from below (configurations a and d). On the other hand, in configurations (b) Down-Up and (c) Up-Up, a temperature of around 410 K is observed, which indicates that the heat would not be uniformly removed in the first step.

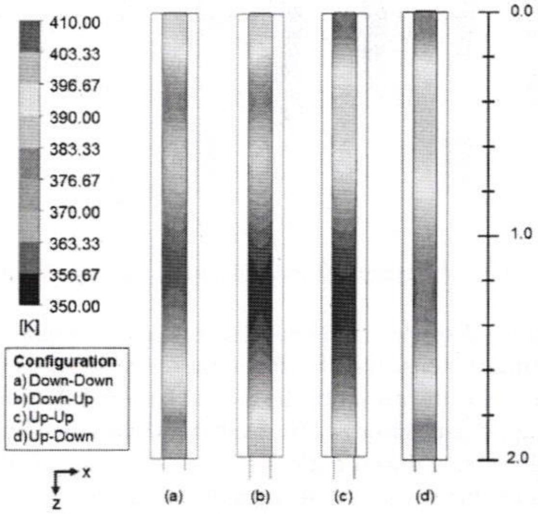

Figure 6. Temperature contours in the flat plate receiver, first pass (Flow 1: 0.01 kg/s).

The existence of a large zone with high temperatures in configurations (a) and (b), between z=0.2 m and z=1.6 m, indicates a low heat removal in the cavity-side plate. In contrast, in configurations (c) and (d), the existence of two well-defined zones of a low and high temperature indicates that although heat removal is heterogeneous, energy is recovered in the zone between z=0.25 m and z=0.8 m. This behavior indicates that the heat obtained by the collector in the first step (inside the cavity) would be lower for the (b) Down-Up configuration.

Table 3 shows the average temperatures in the flat plate receiver ($T_{p,avg}$) for both airflow rates. In the (b) Down-Up configuration, a higher average temperature is reached, and in the (d) Up-Down configuration, the lowest temperatures are achieved, meaning that this configuration favors the heat transfer from the flat-plate to the cavity air. The flat-plate temperature differences between flows 1 and 2 are greater than 40 K.

Table 3. Mean temperatures in the flat plate receiver of the U-shape double-pass CPC.

	Mean Temperature, $T_{p,avg}$ (K)	
Configuration	**Flow 1: 0.01 kg/s**	**Flow 2: 0.02 kg/s**
(a) Down-Down	397.60	353.80
(b) Down-Up	401.40	357.00
(c) Up-Up	404.00	356.60
(d) Up-Down	395.30	352.70

Figure 7 shows the flat plate receiver temperature contours of the four configurations at flow 2 (0.02 kg/s). Here, the exact behavior of temperatures but of lesser magnitude can be observed.

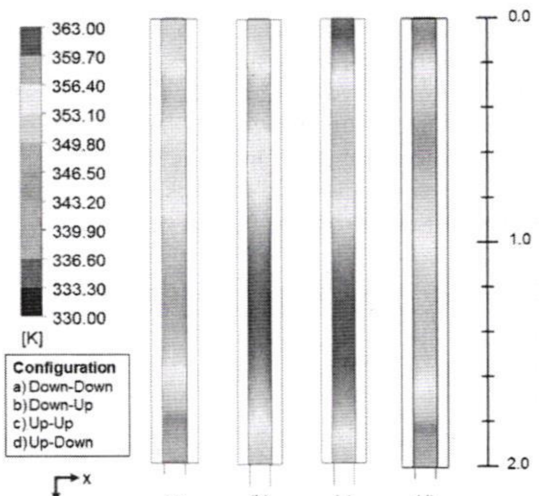

Figure 7. Temperature contours in the flat plate receiver, first pass (Flow 2: 0.02 kg/s).

Figure 8 displays the first and second pass air temperature profiles for the four analyzed configurations. The blue line represents the air temperature profile in the first pass, and the red line the profile of the second pass. In addition, the scale of the horizontal axis of the graphs (z-position) is inverted to facilitate the interpretation of the results since it allows visualizing the air outlet of the collector on the far right.

Besides, in the configurations that have an entrance to the cavity from the top, (c) Up-Up and (d) Up-Down, it is observed that in the first pass, there is a sudden increase in temperature in the section close to the entrance of the cavity (z=0.1 m). On the contrary, in the configurations with the inlet from the bottom, (a) Down-Down and (b) Down-Up, the temperature profile is smooth. In addition, it can be seen that this differentiated profile is more evident in flow 1 (0.01 kg/s).

On the other hand, the configurations that have an outlet from above, (b) Down-Up and (c) Up-Up, present a higher temperature at the outlet end of the cavity (end of the first pass) than at the entrance to the duct (beginning of the second pass). The phenomenon is caused by stratification in the cavity, so the air enters the connecting elbow at a temperature lower than that shown in figure 8 (See Table 4). This occurs with both flows but is more significant with 0.01 kg/s due to the greater air stagnation in the cavity.

The most relevant thing when comparing the four configurations is that the outlet temperature of the second step is between 5 K and 9 K lower in (b) Down-Up than the temperature reached by the other three configurations. Indicating that if the air inlet is located above, i.e., (c) Up-Up or (d) Up-Down, the position of the cavity outlet does not affect the outlet temperature of the collector. However, in the case of bottom entry, (a) Down-Down and (b) Down-Up, configuration (b) would be the least recommended if the objective is to achieve a higher collector outlet temperature.

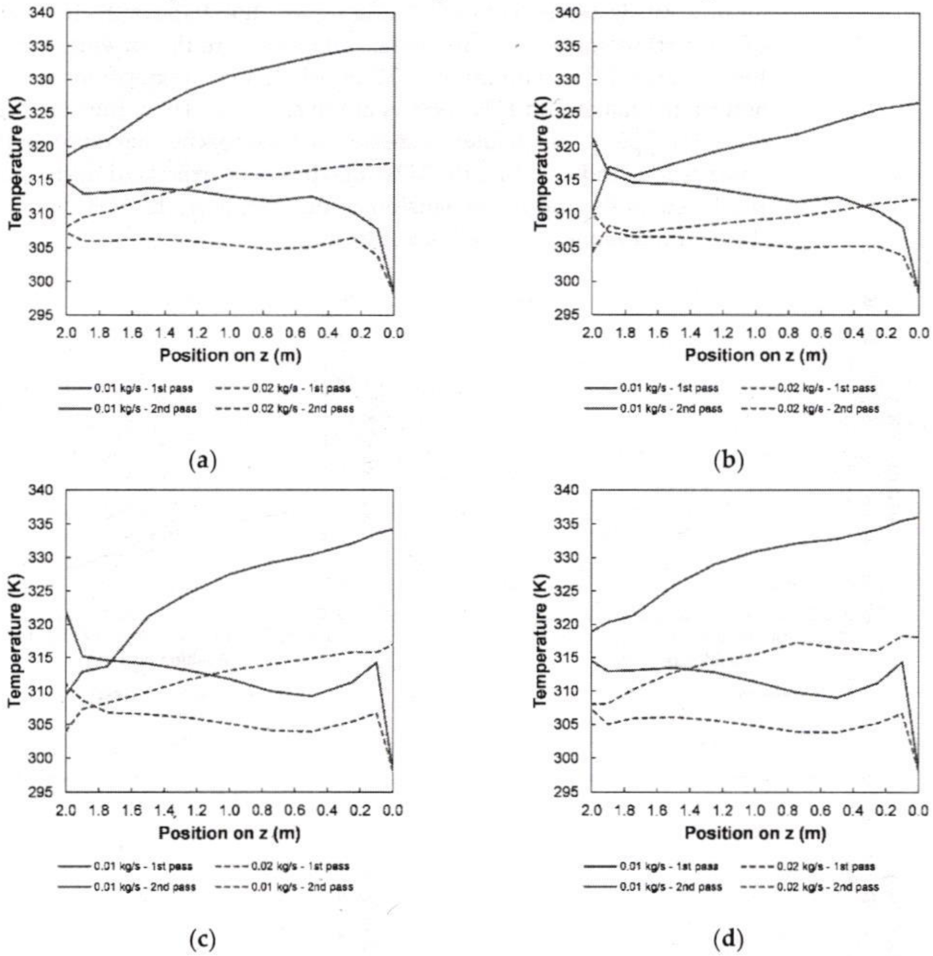

Figure 8. Air temperature profiles. **(a)** Down-Down; **(b)** Down-Up; **(c)** Up-Up; **(d)** Up-Down.

Table 4 shows the elbow inlet and outlet temperatures for both air flow rates. The presented elbow inlet temperature refers to the average temperature at the outlet of the cavity (z=2.0 m) in positions y=0.1255 m to y=0.1645 m, where the height of the elbow is 0.036 m. As expected, the temperatures corresponding to flow 1 (0.01 kg/s) are higher than flow 2 (0.02 kg/s). All of the air temperatures at the elbow inlet are lower than the air temperatures at the outlet of the cavity z=2.0 m. Furthermore, as mentioned above, the fluid is stratified in the cavity, and only the air near the cavity outlet passes through the elbow. On the other hand, the elbow outlet air temperature and the duct inlet air temperature are of the same magnitude.

Table 4. Air temperatures in the elbow inlet and outlet of the U-shape double-pass CPC.

	Flow 1: 0.01 kg/s		Flow 2: 0.02 kg/s	
Configuration	$T_{elb,in}$ (K)	$T_{elb,out}$ (K)	$T_{elb,in}$ (K)	$T_{elb,out}$ (K)
(a) Down-Down	310.5	311.9	304.2	304.9
(b) Down-Up	310.4	311.9	304.2	304.3
(c) Up-Up	311.5	311.8	305.1	304.4
(d) Up-Down	307.1	311.8	302.6	305.2

Figure 9 shows the heat transfer coefficients (HTC) in the cavity for both air flow rates, observing that the HTCs are lower when the airflow is lower and higher when the air flow rate is higher. For each configuration, the shape of the HTC profile is independent of the airflow magnitude. In configurations where the air enters from the top (c and d), there is an HTC maximum at z=0.5 m. While in configurations with inlet from below (a and b), the maximum HTC occurs at the entrance. Then, the HTC decreases, having another HTC peak, which later decreases as it approaches the outlet of the cavity. The above observations indicate that the HTC maximums correspond to the presence of the eddies produced by the sudden expansion at the inlet; here, the HTC is of greater magnitude in the configurations with the inlet at the top.

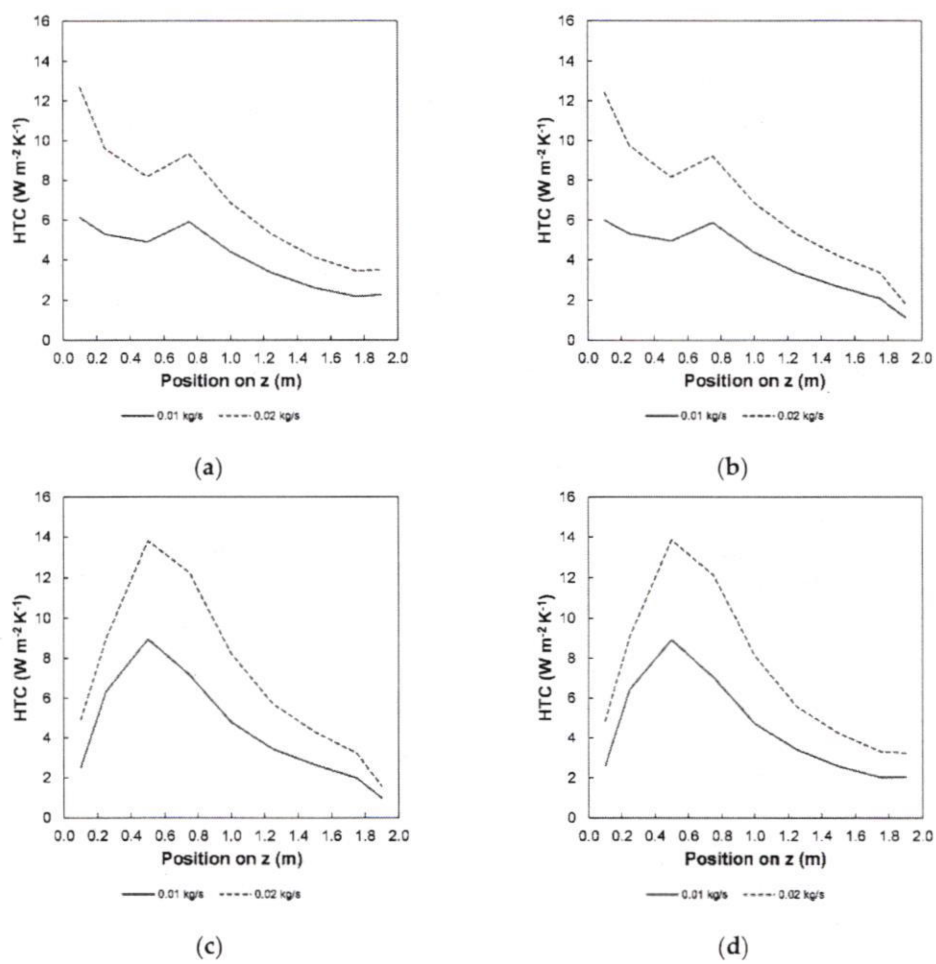

Figure 9. Flat-plate receiver heat transfer coefficients (HTC). **(a)** Down-Down; **(b)** Down-Up; **(c)** Up-Up; **(d)** Up-Down.

Table 5 shows the pressure drop in each configuration for the two mass flow rates. First, the highest pressure drop is seen in the bottom outlet configurations (a and d). Moreover, the pressure drop increases three to four times with the highest air flow rate.

Table 5. Pressure drop in the system.

	Pressure drop (Pa)	
Configuration	**Flow 1: 0.01 kg/s**	**Flow 2: 0.02 kg/s**
(a) Down-Down	9.87	35.49
(b) Down-Up	8.00	28.79
(c) Up-Up	8.42	29.52
(d) Up-Down	10.05	36.17

3.3. *Efficiency*

Table 6 shows the temperature increment in the first pass and the efficiencies for each configuration, applying equations (16) and (17). The temperature increase resulting from the first pass (ΔT_{p1}) and the temperatures at the inlet and outlet of the duct ($T_{p2,in}$ and $T_{p2,out}$) are greater with flow 1, while the efficiencies are higher with flow 2 due to the better heat transfer and lower heat losses to the ambient. In addition, it is observed that configuration (c) Up-Up is the most efficient, while configuration (a) Down-Down provides the lower efficiency of the cases analyzed.

Table 6. U-shape double-pass CPC thermal efficiency ($T_{f1,in}$=298.15 K)

	Flow 1: 0.01 kg/s				**Flow 2: 0.02 kg/s**			
Configuration	**ΔT_{ps1} (K)**	**$T_{ps2,in}$ (K)**	**$T_{ps2,out}$ (K)**	**η (%)**	**ΔT_{ps1} (K)**	**$T_{ps2,in}$ (K)**	**$T_{ps2,out}$ (K)**	**η (%)**
(a) Down-Down	13.75	311.90	333.80	60.71	6.75	304.90	316.10	61.91
(b) Down-Up	13.75	311.90	335.20	64.60	6.15	304.30	317.10	70.76
(c) Up-Up	13.65	311.80	336.60	68.77	6.25	304.40	317.40	71.87
(d) Up-Down	13.65	311.80	335.40	65.43	7.05	305.20	317.30	66.90

4. Conclusions

This work investigates a compound parabolic concentrator (CPC) design for air heating with a double U-pass configuration. The double pass is incorporated to recover part of the heat lost by the flat plate receiver inside the CPC cavity. Four configurations have been studied, and they are differentiated by the position of the air inlet into the cavity and the position of the air outlet of the cavity towards the receiving duct that constitutes the second pass of the collector.

In general, it was confirmed that adding the first pass through the CPC cavity allows a significant increase in the air temperature. Hence, by making the air circulate first through the CPC cavity, instead of a conventional manner where it only circulates through the duct, an increase in temperature is accomplished before entering the receiving duct. As a result, an average increase in air temperature of 13.7 K at a mass flow rate of 0.01 kg/s and 6.5 K at a mass flow rate of 0.02 kg/s was achieved. This represents a minimum temperature rise of 36 % (0.01 kg/s) and 32 % (0.02 kg/s) when only the first pass is used.

In addition, the analysis showed that the positions of the air inlet and outlet in the cavity influence the outlet temperature of the U-shape double pass CPC solar heater. Therefore, an efficiency difference of up to 10 % can be achieved depending on the selected configuration. Thus, the Up-Up configuration is the one that provides the highest outlet temperature and thermal efficiency. With this configuration, an air temperature increase from the U-shape double-pass CPC inlet to the outlet of 38.4 K and an efficiency of 68.9 % are obtained when the air flow rate is 0.01 kg/s, and 19.2 K and 71.9 % when the flow rate is 0.02 kg/s. This is because the air heated in the cavity is transported more effectively, as it is a more homogeneous flow and the heat transfer coefficient in the flat-plate receiver is high.

However, it should be noted that the Down-Down (a) configuration can be ruled out because it has the smallest increase in temperature and the lowest efficiency of the analyzed configurations.

Finally, the structural design and financial analysis remain as future work to determine the potential application of this technology. The Down-Up (b) or Up-Down (d) configurations could also be used depending on the application conditions and specific needs.

Author Contributions: Conceptualization, Irving Chávez-Bermúdez, Eduardo Venegas-Reyes and Naghelli Ortega-Avila; Data curation, Irving Chávez-Bermúdez; Formal analysis, Irving Chávez-Bermúdez, Norma Rodríguez-Muñoz, Loreto Valenzuela and Naghelli Ortega-Avila; Funding acquisition, Naghelli Ortega-Avila; Investigation, Irving Chávez-Bermúdez; Methodology, Irving Chávez-Bermúdez and Norma Rodríguez-Muñoz; Project administration, Naghelli Ortega-Avila; Resources, Norma Rodríguez-Muñoz; Software, Irving Chávez-Bermúdez; Supervision, Norma Rodríguez-Muñoz, Eduardo Venegas-Reyes and Naghelli Ortega-Avila; Validation, Irving Chávez-Bermúdez and Norma Rodríguez-Muñoz; Visualization, Irving Chávez-Bermúdez, Norma Rodríguez-Muñoz and Naghelli Ortega-Avila; Writing – original draft, Irving Chávez-Bermúdez, Norma Rodríguez-Muñoz and Naghelli Ortega-Avila; Writing – review & editing, Irving Chávez-Bermúdez, Norma Rodríguez-Muñoz, Eduardo Venegas-Reyes, Loreto Valenzuela and Naghelli Ortega-Avila.. All authors have read and agreed to the published version of the manuscript.

Funding: The APC was funded by the Centro de Investigacion en Materiales Avanzados (CIMAV) through project number PI-22-24.

Data Availability Statement: Not applicable.

Acknowledgments: The authors wish to thank the Mexican National Science Council (CONACYT) for the financial support through the scholarship 698432. To Durango Science and Technology Council (COCYTED) for the financing of the annual ANSYS software license. Also, to the Laboratorio de Computo Cientifico of FCQ-UJED and the Academic Group UJEDCA129 for the use of software and computational facilities.

Conflicts of Interest: The authors declare no conflict of interest. The funders had no role in the design of the study; in the collection, analyses, or interpretation of data; in the writing of the manuscript; or in the decision to publish the results.

Nomenclature

$\langle n \rangle$	Average reflections number, dimensionless
A	Area, m^2
C	Constant
C_p	Specific heat, J/(kg K)
D_h	Hydraulic diameter, m
E	Relaminarization source
F	Empirical correlation of length of the transition region, m
$\vec{F}$	Force vector, N
$\vec{g}$	Gravitational acceleration, m/s^2
G_k	Generation of turbulence kinetic energy due to mean velocity gradients, J/kg
G_w	Generation of specific dissipation rate, 1/s
h	Height, m
h'	Species enthalpy, J/kg
I	Solar irradiance, W/m^2
J	Mass flux, kg/m^2
k	Turbulent kinetic energy, J
L	Length, m
$\dot{m}$	Mass flow rate, kg/s

Nu	Nusselt number, dimensionless
P	Pressure, Pa
P_g	Gap loss factor, dimensionless
q	Heat generation, W/m^3
Q_u	Useful heat, W
Re	Reynolds number, dimensionless
S	Strain rate magnitude
t	Time, s
T	Temperature, K
u	Velocity magnitude, m/s
U	Local velocity, m/s
u_T	Friction velocity, m/s
V	Free-stream speed, m/s
v	Wind velocity above cover, m/s
w	Width, m
x	Velocity field coordinate
y	Wall-normal distance, m
Y	Destruction term of SST turbulence model, m^2/s^3
y+	Dimensionless distance in wall coordinates

Greek letters

α	Absorptance, dimensionless
γ	Intermittency
Γ	Effective diffusivity, dimensionless
ε	Emittance, dimensionless
η	Thermal efficiency, dimensionless
μ	Molecular viscosity of air, kg/(m s)
ρ	Air density, kg/m^3
ϱ	Reflectance, dimensionless
τ	Transmittance, dimensionless
$\bar{\bar{\tau}}$	Stress tensor, Pa
υ	Eddy viscosity
Ω	Vorticity magnitude, 1/s

Subscripts

a	Ambient
a1, a2	Turbulence damping constants
ap	Aperture
avg	Average
b	Bottom duct
c	Cover
cav	Cavity
collector	Collector
duct	Duct
elb	Elbow
e1, e2	Dissipation
h	Hydrodynamic
i, j	Orthogonal coordinate
in	Inlet
k	Turbulence kinetic energy
length	Length
out	Outlet

p	Flat plate receiver
ps1	Pass 1 (Through the cavity)
ps2	Pass 2 (Through the duct)
r	Reflectors
s	Sky
turb	Turbulent
$\gamma1$, $\gamma2$	Intermittence

Acronyms

CFD	Computational fluid dynamics
CPC	Compound parabolic concentrator
EPS	Expanded polystyrene
ETFE	Ethylene tetrafluoroethylene (fluorine-based plastic)
HTC	Heat transfer coefficient, W/(m^2 K)
PV/T	Photovoltaic/Thermal

References

1. Weiss, W.; Spörk-Dür, M. Solar Heat World 2022. Global Market Development and Trends 2021. Detailed Market Figures 2020 2022, 87.
2. Bhusal, Y.; Hassanzadeh, A.; Jiang, L.; Winston, R. Technical and Economic Analysis of a Novel Low-Cost Concentrated Medium-Temperature Solar Collector. *Renew. Energy* **2020**, *146*, 968–985, doi:10.1016/j.renene.2019.07.032.
3. Buttinger, F.; Beikircher, T.; Pröll, M.; Schölkopf, W. Development of a New Flat Stationary Evacuated CPC-Collector for Process Heat Applications. *Sol. Energy* **2010**, *84*, 1166–1174, doi:10.1016/j.solener.2010.03.022.
4. Horta, P.; Henriques, J.C.C.; Collares-Pereira, M. Impact of Different Internal Convection Control Strategies in a Non-Evacuated CPC Collector Performance. *Sol. Energy* **2012**, *86*, 1232–1244, doi:10.1016/j.solener.2012.01.016.
5. Zheng, W.; Yang, L.; Zhang, H.; You, S.; Zhu, C. Numerical and Experimental Investigation on a New Type of Compound Parabolic Concentrator Solar Collector. *Energy Convers. Manag.* **2016**, *129*, 11–22, doi:10.1016/j.enconman.2016.10.013.
6. Nkwetta, D.N.; Smyth, M. Performance Analysis and Comparison of Concentrated Evacuated Tube Heat Pipe Solar Collectors. *Appl. Energy* **2012**, *98*, 22–32, doi:10.1016/j.apenergy.2012.02.059.
7. Alam, T.; Kim, M.-H. A Critical Review on Artificial Roughness Provided in Rectangular Solar Air Heater Duct. *Renew. Sustain. Energy Rev.* **2017**, *69*, 387–400, doi:10.1016/j.rser.2016.11.192.
8. Hj. Othman, M.Y.; Yatim, B.; Sopian, K.; Abu Bakar, M.N. Performance Analysis of a Double-Pass Photovoltaic/Thermal (PV/T) Solar Collector with CPC and Fins. *Renew. Energy* **2005**, *30*, 2005–2017, doi:10.1016/j.renene.2004.10.007.
9. Mekahlia, A.; Boumaraf, L.; Abid, C. CFD Analysis of the Thermal Losses on the Upper Part of a Flat Solar Collector. *Heat Transf.* **2020**, *49*, 2921–2942, doi:10.1002/htj.21753.
10. Pawar, V.R.; Sobhansarbandi, S. CFD Modeling of a Thermal Energy Storage Based Heat Pipe Evacuated Tube Solar Collector. *J. Energy Storage* **2020**, *30*, 101528, doi:10.1016/j.est.2020.101528.
11. Singla, M.; Hans, V.S.; Singh, S. CFD Analysis of Rib Roughened Solar Evacuated Tube Collector for Air Heating. *Renew. Energy* **2022**, *183*, 78–89, doi:10.1016/j.renene.2021.10.055.
12. Ammar, M.; Mokni, A.; Mhiri, H.; Bournot, P. Numerical Analysis of Solar Air Collector Provided with Rows of Rectangular Fins. *Energy Reports* **2020**, *6*, 3412–3424, doi:10.1016/j.egyr.2020.11.252.
13. Li, X.; Dai, Y.J.; Li, Y.; Wang, R.Z. Performance Investigation on a Novel Single-Pass Evacuated Tube with a Symmetrical Compound Parabolic Concentrator. *Sol. Energy* **2013**, *98*, 275–289, doi:10.1016/j.solener.2013.10.015.
14. Barrón-Díaz, J.E.; Flores-Johnson, E.A.; Chan-Colli, D.G.; Koh-Dzul, J.F.; Bassam, A.; Patiño-Lopez, L.D.; Carrillo, J.G. FEM-CFD Simulation and Experimental Study of Compound Parabolic Concentrator (CPC) Solar Collectors with and without Fins for Residential Applications. *Appl. Sci.* **2021**, *11*, 3704, doi:10.3390/app11083704.

15. Yuan, G.; Fan, J.; Kong, W.; Furbo, S.; Perers, B.; Sallaberry, F. Experimental and Computational Fluid Dynamics Investigations of Tracking CPC Solar Collectors. *Sol. Energy* **2020**, *199*, 26–38, doi:10.1016/j.solener.2020.01.090.
16. Antonelli, M.; Francesconi, M.; Di Marco, P.; Desideri, U. Analysis of Heat Transfer in Different CPC Solar Collectors: A CFD Approach. *Appl. Therm. Eng.* **2016**, *101*, 479–489, doi:10.1016/j.applthermaleng.2015.12.033.
17. Francesconi, M.; Antonelli, M. A CFD Analysis to Investigate Thermal Losses in a Panel Composed of Several CPC Concentrators. *Therm. Sci. Eng. Prog.* **2018**, *5*, 278–288, doi:10.1016/j.tsep.2017.12.005.
18. Reddy, K.S.; Parthiban, A.; Mallick, T.K. Numerical Modeling of Heat Losses in a Line Focusing Solar Compound Parabolic Concentrator with Planar Absorber. *Appl. Therm. Eng.* **2020**, *181*, 115938, doi:10.1016/j.applthermaleng.2020.115938.
19. Al-Damook, M.; Obaid, Z.A.H.; Al Qubeissi, M.; Dixon-Hardy, D.; Cottom, J.; Heggs, P.J. CFD Modeling and Performance Evaluation of Multipass Solar Air Heaters. *Numer. Heat Transf. Part A Appl.* **2019**, *76*, 438–464, doi:10.1080/10407782.2019.1637228.
20. Tuncer, A.D.; Sözen, A.; Khanlari, A.; Amini, A.; Şirin, C. Thermal Performance Analysis of a Quadruple-Pass Solar Air Collector Assisted Pilot-Scale Greenhouse Dryer. *Sol. Energy* **2020**, *203*, 304–316, doi:10.1016/j.solener.2020.04.030.
21. Mutabilwa, P.X.; Nwaigwe, K.N. Experimental Evaluation of Drying of Banana Using a Double-Pass Solar Collector (DPSC) and Theoretical Analysis Using a CFD Model. *Cogent Eng.* **2020**, *7*, 1789363, doi:10.1080/23311916.2020.1789363.
22. Desisa, D.G.; Shekata, G.D. Performance Analysis of Flat-Plate and V-Groove Solar Air Collector through CFD Simulation. *Int. J. Renew. Energy Dev.* **2020**, *9*, 369–381, doi:10.14710/ijred.2020.30091.
23. Singh, S. Thermohydraulic Performance of Double Pass Solar Thermal Collector with Inline, Staggered and Hybrid Fin Configurations. *J. Energy Storage* **2020**, *27*, 101080, doi:10.1016/j.est.2019.101080.
24. Kumar, A.; Singh, A.P.; Akshayveer; Singh, O.P. Performance Characteristics of a New Curved Double-Pass Counter Flow Solar Air Heater. *Energy* **2022**, *239*, 121886, doi:10.1016/j.energy.2021.121886.
25. Chávez-Bermúdez, I.A.; Ortega-Avila, N.; Venegas-Reyes, E. A Thermal Model for a CPC-Type Double-Pass Solar Air Heater. In Proceedings of the AIP Conference Proceedings; 2022; Vol. 2445, p. 120007.
26. Menter, F.R.; Langtry, R.B.; Likki, S.R.; Suzen, Y.B.; Huang, P.G.; Völker, S. A Correlation-Based Transition Model Using Local Variables—Part I: Model Formulation. *J. Turbomach.* **2006**, *128*, 413, doi:10.1115/1.2184352.
27. Santos-González, I.; García-Valladares, O.; Ortega, N.; Gómez, V.H. Numerical Modeling and Experimental Analysis of the Thermal Performance of a Compound Parabolic Concentrator. *Appl. Therm. Eng.* **2017**, *114*, 1152–1160, doi:10.1016/j.applthermaleng.2016.10.100.
28. Rabl, A. Optical and Thermal Properties of Compound Parabolic Concentrators. *Sol. Energy* **1976**, *18*, 497–511, doi:10.1016/0038-092X(76)90069-4.
29. Duffie, J.A.; Beckman, W.A. *Solar Engineering of Thermal Processes*; John Wiley & Sons, Inc.: Hoboken, NJ, USA, 2013; ISBN 9781118671603.
30. ISO/TC 180 Solar energy Solar Energy — Solar Thermal Collectors — Test Methods 2017, 90.

GOBIERNO DE MÉXICO | CONACYT Consejo Nacional de Ciencia y Tecnología | cimav

September 22th 2022

Dear Editor
Applied Sciences
MDPI

We would like to submit for publication the attached paper entitled "Thermal performance analysis of a double-pass solar air collector: A CFD approach" by Irving A. Chávez-Bermúdez, Norma A. Rodríguez-Muñoz, Eduardo Venegas-Reyes, Loreto Valenzuela and Naghelli Ortega-Avila to the Applied Sciences Journal.

The content in the document fits the Applied Sciences Journal Research topic "Advances in Renewable Energy and Energy Storage" as it presents an investigation of the thermal performance of a U-shape double pass solar heater with drying and space heating applications. The investigation carries out a CFD analysis of a CPC-type solar air heater to test different inlet and outlet configurations and a calculation of the efficiency alternative to the presented in the ISO 9806.

Finally, we confirm that neither the manuscript nor any parts of its content are currently under consideration or published in another journal. All authors have approved the manuscript and agree with its submission to Applied Sciences.

We look forward to hearing from you.

Dr. Naghelli Ortega Avila
Investigadora por México - CONACYT
Centro de Investigación en Materiales Avanzados, S. C.
Durango, México
Email: naghelli.ortega@cimav.edu.mx

CentroM de Investigación en Materiales Avanzados S. C.

FECHA ELABORACIÓN: **27 de septiembre de 2022**

ASUNTO: ESTUDIO DE MERCADO

No. Partida / CUCOP
21502 MATERIAL PARA INFORMACIÓN EN ACTIVIDADES DE INVESTIGACIÓN CIENTÍFICA Y TECNOLÓGICA

No. Requisición
221054

Descripción

Publicación de artículo en revista JCR de MDPI - Manuscript ID: applsci-1958428 (Entregable del proyecto)

Proveedores

1) MDPI

Precio: CHF2,300.00 CHF Origen del bienExtranjero Fuente de consultaInternet

Cumplimiento de condiciones técnicas:
Sí

Cantidad que puede surtir:
1

ELABORÓ
NAJERA TREJO MARIO

Centro de Investigación en Materiales Avanzados S. C.

JUSTIFICACIÓN PARA ACREDITAR Y FUNDAR PROCEDIMIENTOS DE CONTRATACION POR ADJUDICACION DIRECTA, COMO EXCEPCION AL DE LICITACION PUBLICA EN EL SUPUESTO DEL ARTICULO 41 FRACCION I DE LA LEY DE ADQUISICIONES, ARRENDAMIENTOS Y SERVICIO EN EL SECTOR PUBLICO.

COMITÉ DE ADQUISICIONES, ARRENDAMIENTOS Y SERVICIOS

PRESENTE:

Oficio número: **221054**

Asunto: Se emite la justificación por la que se acredita y funda la contratación por adjudicacion directa que se indica.

En cumplimiento a lo establecido en el segundo párrafo del artículo 40 de la Ley de Adquisiciones, Arrendamientos y Servicios del Sector Público, así como en el artículo 71 del Reglamento de la Ley de Adquisiciones, Arrendamientos y Servicios del Sector Público, y con el carácter de Titular del Área Requirente, por este conducto hago constar el acreditamiento del o de los criterios, razones, fundamentos y motivos para no llevar a cabo el procedimiento de licitación pública y celebrar la contratación a través del procedimiento de adjudicación directa en los términos establecidos en el artículo 41 Fracción I de la Ley de Adquisiciones, Arrendamientos y Servicios del Sector Público

Para tal efecto presento la siguiente información:

I.- DESCRIPCIÓN DE LOS SERVICIOS

El/Los servicios que se pretende contratar, son los siguientes:

Publicación de artículo en revista JCR de MDPI - Manuscript ID: applsci-1958428 (Entregable del proyecto)

II.- PLAZOS Y CONDICIONES DEL SUMINISTRO DE LOS SERVICIOS

La fecha en que se requiere el suministro de los servicios, corresponde al día **31 de octubre de 2022**. Las condiciones en las que se entregarán los servicios son las siguientes:

En una sola exhibición

Virtual a través del portal de la revista JCR

III.- RESULTADO DE LA INVESTIGACIÓN DE MERCADO

La Investigación de Mercado fue realizada en los términos de los artículos 28, 29 y 30 del Reglamento de la Ley de Adquisiciones, Arrendamientos y Servicios del Sector Público, en forma conjunta por el Área Requirente y el Área Contratante, en la cual se verificó previo alinicio del procedimiento de contratación, la existencia de oferta, en la cantidad, calidad y oportunidad requeridas; la existencia de proveedores a nivel nacional o internacional con posibilidad de cumplir con las necesidades de la contratación, conocer el precio prevaleciente al momento de llevar a cabo la Investigación de mercado así como en la información disponible en el Sistema informático denominado COMPRANET:

PROVEEDOR	IMPORTE SIN IVA
MDPI	CHF2,300.00 CHF

Concluyendo que en conjunto es la única oferta en cuanto a obtener las mejores condiciones, calidad, precio, oportunidad y financiamiento, por ser el único proveedor que proporcione los servicios que se pretende contratar la de **MDPI**. La referida Investigación de Mercado se acompaña a la presente justificación para determinar que el procedimiento de contratación por adjudicación directa es el idóneo.

IV.- PROCEDIMIENTO DE CONTRATACIÓN PROPUESTO

El procedimiento de contratación propuesto es el de adjudicación directa, en virtud de que en el presente caso la adjudicación se llevaría a cabo conforme la fracción I del artículo 41 el cual menciona que este tipo de adjudicación se puede llevar a cabo siempre y cuando: **No existan bienes o servicios alternativos o sustitutos técnicamente razonables, o bien, que en el mercado sólo existe un posible oferente, o se trate de una persona que posee la titularidad o el licenciamiento exclusivo de patentes, derechos de autor, u otros derechos exclusivos, o por tratarse de obras de arte.** Actualizándose el supuesto de excepción a la licitación pública establecido en la fracción I del artículo 41 de la Ley de Adquisiciones, Arrendamientos y Servicios del Sector Público, en relación con lo establecido en el artículo 72 de su Reglamento.

IV.1. MOTIVACIÓN Y FUNDAMENTACIÓN LEGAL:

A) MOTIVOS: La contratación de los servicios objeto de la presente justificación es necesaria para satisfacer los siguientes requerimientos del proyecto número **24024 - DESARROLLO DE UN CALENTADOR SOLAR DE AIRE DE** : Se requiere pagar el acceso abierto por la publicación del artículo en extenso en la revista Applied Science de MDPI que es un entregable del proyecto. En este artículo se publican los resultados del análisis en CFD de la transferencia de calor en el calentador solar de aire de doble paso desarrollado, y se determina la influencia, en la eficiencia y temperatura alcanzadas, de la ubicación de la entrada y de la salida de la cavidad. .

Por lo anterior, la contratación propuesta se adecúa al supuesto de excepción establecido en la Ley de Adquisiciones, Arrendamientos y Servicios del Sector Público en su artículo 41, fracción I; además de que se reúnen los requisitos previstos en el artículo 72 del Reglamento de la Ley de Adquisiciones, Arrendamientos y Servicios del Sector Público, tal y como se desprende de la información presentada en esta justificación, así como de la Investigación de Mercado; por lo que resulta procedente la contratación bajo el procedimiento de adjudicación directa previsto en el artículo 26, fracción III de la Ley antes mencionada.

B) FUNDAMENTOS: La contratación se encuentra debidamente fundada en el artículo 134 de la Constitución Política de los Estados Unidos Mexicanos; en los artículos 26 fracción III, 40 y 41 fracción I de la Ley de Adquisiciones, Arrendamientos y Servicios del Sector Público; así como en los artículos 71 del Reglamento de la Ley de Adquisiciones, Arrendamientos y Servicios del Sector Público.

IV.-MONTO ESTIMADO Y FORMA DE PAGO PROPUESTO

V.1. MONTO ESTIMADO:

El monto estimado de la contratación es la cantidad de **CHF2,300.00 CHF**, mismo resultó el más conveniente de acuerdo con la Investigación de Mercado, mediante la cual se verificó previo al inicio del procedimiento de contratación, la existencia de oferta de los servicios en la cantidad, calidad y oportunidad requeridos en los términos del artículo 28 del Reglamento de la Ley de Adquisiciones, Arrendamientos y Servicios del Sector Público.

SubTotal:	CHF2,300.00 CHF
Iva:	CHF0.00 CHF
Total:	**CHF2,300.00 CHF**

V.2. FORMA DE PAGO PROPUESTA:

El monto total será pagado en **1 pago/s de CHF2,300.00 CHF**. Los pagos se realizarán previa verificación de la entrega y calidad de los servicios así como previo envío en formatos .pdf y .xml del Comprobante Fiscal Digital por Internet (CFDI) correspondiente que reúna los requisitos fiscales respectivos. Los pagos se efectuarán mediante TRANSFERENCIA y bajo las siguientes condiciones:

Segun referencia

IV.-PROVEEDOR PROPUESTO PARA LA ADJUDICACIÓN DIRECTA:

Por lo anteriormente expuesto y fundado, se propone a MDPI, con domicilio ubicado en ST ALBAN-ANLAGE 66, 4052 BASEL, SWITZERLAND, Registro Federal de Contribuyentes: XEXX4162, correo electrónico: billing@mpdi.com y número telefónico 41616837734, 41616837734

VII.- ACREDITAMIENTO DEL O LOS CRITERIOS EN LOS QUE SE FUNDA Y MOTIVA LA SELECCIÓN DEL PROCEDIMIENTO DE EXCEPCIÓN A LA LICITACIÓN PÚBLICA:

El procedimiento de contratación por adjudicación directa es el idóneo, al actualizarse el supuesto de excepción al procedimiento de licitación pública previsto en el artículo 41, fracción I de la Ley de Adquisiciones, Arrendamientos y Servicios del Sector Público, aunado a que se corroboró la capacidad y experiencia de la persona propuesta, quien presentó las mejores condiciones en cuanto a precio, calidad, financiamiento, oportunidad y demás circunstancias pertinentes a efecto de asegurar a esta Entidad las mejores condicionespara su contratación, tal y como se acredita con la información presentada en esta justificación, así como con la Investigación de Mercado.

El acreditamiento del o los criterios en los que se funda la excepción de licitación pública, es el o los siguientes:

- Economía
Se efectuó una investigación de mercado para comparar precios y demás condiciones de calidad, financiamiento y oportunidad, respecto del bien requerido, dando como resultado que la persona moral propuesta, fue la que presentó las mejores condiciones en cuanto a precio, calidad, financiamiento y oportunidad, con lo cual se asegura cumplir con los preceptos del Artículo 134 de la Constitución Política de los Estados Unidos Mexicanos; así como en los Artículos 40 y 41, fracción XVII de la Ley de Adquisiciones, Arrendamientos y Servicios del Sector Público, por lo que resulta adecuado proceder a la adjudicación directa a favor del proveedor antes referido.

- Eficacia
Mediante el procedimiento de adjudicación directa, se conseguirán las mejores condiciones disponibles para la Entidad en cuanto a precio, calidad, y oportunidad, en adición a que el Proveedor propuesto cuenta con la experiencia y capacidad idóneas para suministrar el bien requerido, y con ello se lograrán los objetivos y resultados deseados

- Eficiencia
Con el procedimiento de adjudicación propuesto se garantizan las mejores condiciones de precio, calidad, oportunidad y demás circunstancias pertinentes debido a que se optimiza el uso y aplicación de los recursos financieros, en virtud de que esta Entidad cuenta con procesos y procedimientos claros y expeditos, con responsables y responsabilidades plenamente identificados para la contratación requerida, con lo cual se evitará la pérdida de tiempo y recursos a la Entidad.

- Imparcialidad
El tipo de adjudicación que se propone, se llevó a cabo sin prejuicios ni situaciones que pudieran afectar la imparcialidad, y sin que medie algún interés personal de los servidores públicos involucrados en la contratación de cualquier otra índole que pudiera otorgar condiciones ventajosas a alguna persona, en relación con los demás ni limitar la libre participación, esto debido a que es proveedor único,dicha situación queda demostrada conforme al resultado que se da con base a la investigación de mercado. Lo anterior de acuerdo con lo establecido en el numeral 4.2.4 (ADJUDICACIÓN DIRECTA) y numeral 4.2.4.1.1 (Verificar acreditamiento de excepción) del Acuerdo por el que se expide el Manual Administrativo de Aplicación General en Materia de Adquisiciones, Arrendamientos Servicios del Sector Público, publicado en el Diario Oficial de la Federación el 9 de agosto de 2010, última reforma publicada el 3 de febrero de 2016 en el Diario Oficial de la Federación.

- Honradez
La selección del procedimiento de adjudicación directa tiene como único fin contratar bajo las mejores condiciones los servicios requeridos actuando con rectitud responsabilidad e integridad y con apego estricto al marco jurídico aplicable, evitando así incurrir en actos de corrupción y conflictos de interés, ya que con base a la investigación de mercado queda demostrado que es proveedor único.

Lo anterior de acuerdo con lo establecido en el numeral 4.2.4 (ADJUDICACIÓN DIRECTA) y numeral 4.2.4.1.1 (Verificar acreditamiento de excepción) del Acuerdo por el que se expide el Manual Administrativo de Aplicación General en Materia de Adquisiciones, Arrendamientos Servicios del Sector Público, publicado en el Diario Oficial de la Federación el 9 de agosto de 2010, última reforma publicada el 3 de febrero de 2016 en el Diario Oficial de la Federación.

- Transparencia
Para la integración del procedimiento de contratación por adjudicación directa, los servidores públicos de las áreas requirentes han tenido acceso de manera oportuna, clara y completa de las características requeridas de los servicios con el fin de demostrar que es el único proveedor que proporciona los servicios que se pretenden contratar, en el entendido que para garantizar la transparencia del procedimiento de contratación, la información respectiva será incorporada al Sistema de Compras Gubernamentales (CompraNet), en los términos de las disposiciones legales aplicables, Lo anterior de acuerdo con lo establecido en el numeral 4.2.4 (ADJUDICACIÓN DIRECTA) y numeral 4.2.4.1.1 (Verificar acreditamiento de excepción) del Acuerdo por el que se expide el Manual Administrativo de Aplicación General en Materia de Adquisiciones, Arrendamientos y Servicios del Sector Público, publicado en el Diario Oficial de la Federación el 9 de agosto de 2010, última reforma publicada el 3 de febrero de 2016 en el Diario Oficial de la Federación.

VIII.- LUGAR Y FECHA DE EMISIÓN:

En la Ciudad de Chihuahua, Chihuahua al **29 de septiembre de 2022**, se emite la presente justificación para los efectos legales a que haya lugar.

En cumplimiento a lo establecido en el penúltimo párrafo del artículo 71 del Reglamento de la Ley de Adquisiciones, Arrendamientos y Servicios del Sector Público, se acompaña a la presente como "ANEXO DOS", la Requisición o Solicitud de Contratación (Requisición) A la cual se deberá anexar, mediante sello del departamento de Presupuesto, la Constancia con la que se acredita la existencia de recursos para iniciar el procedimiento de contratación.

Asimismo se hace constar mediante el sello y firma del responsable del área de Almacén, la No Existencia de Bienes o Nivel de Inventario que demuestra que se cumplió con lo establecido en el artículo 27 del RLAASP.

ATENTAMENTE

MARTIN DOMINGUEZ IGNACIO RAMIRO
RESPONSABLE DEL PROYECTO